Feasibility study of indocyanine green for visualizing malignant lesions in colitis-associated colorectal cancer patients with real-time fluorescence endoscopy

Jinhyeon Kim
University of Ulsan College of Medicine
Hajung Kim
Asan Medical Center
Yong Sik Yoon
University of Ulsan College of Medicine
Chan Wook Kim
University of Ulsan College of Medicine
Seung-Mo Hong
University of Ulsan College of Medicine
Sungjee Kim
Pohang University of Science & Technology
Doowon Choi
Pohang University of Science & Technology
Jihyun Chun
University of Ulsan College of Medicine
Jeong-Sik Byeon
University of Ulsan College of Medicine
Byong Duk Ye
University of Ulsan College of Medicine
Suk-Kyun Yang
University of Ulsan College of Medicine
Sun Young Kim (enthalpy98@gmail.com)
University of Ulsan College of Medicine
Seung-Jae Myung
University of Ulsan College of Medicine

Article

Keywords:

Posted Date: June 10th, 2022

DOI: https://doi.org/10.21203/rs.3.rs-1671796/v1

Abstract

Indocyanine green (ICG) has been used in clinical practice for more than 40 years and its safety and preferential accumulation of ICG in tumors has been reported for various tumor types, including colon cancer. However, reports on the clinical assessments of ICG-based molecular endoscopy imaging for pre-cancerous lesions are scarce. Therefore, we determined the percent visualization ability of ICG endoscopy in colitis-associated colon cancer using 30 lesions from an animal model and 16 patient tissues. ICG could detect 100% of carcinoma, 90% adenoma, and 57.1% dysplasia, with little background signal at 30 min after injection via real-time fluorescence endoscopy. Correlation analysis of ICG fluorescence intensity and cancer specific molecules revealed a positive correlation of ICG with c-Met and iNOS ($r > 0.5$). A high level of iNOS expression increased the cellular nitric oxide in cancer cells than that in normal cells, which was related to the inhibition of drug efflux via ABCB1 transporter down regulation resulted to delayed retention of intracellular ICG. These findings highlight the feasibility of ICG as a detector of pre-cancerous lesions in real-time fluorescence endoscopy and suggest that the mechanism of ICG retention in cancer cells is related with intracellular nitric oxide concentration.

Introduction

Colorectal cancer (CRC) is the most common cancer worldwide and the leading cause of cancer-related deaths[1]. The progression of adenoma leads to CRC, and this progression involves the conventional tubular adenoma pathway and the alternative serrated polyp pathway[2]. Chronic inflammation is a major risk factor that induces different morphologies and dysplasia-carcinoma progression in patients with inflammatory bowel disease (IBD)[3]. Hence, the detection of early phase cancer or dysplasia as a precancerous lesion could lead to decreased mortality.

Currently, white-light endoscopy is the gold standard for screening colonoscopy; however, the miss rate of endoscopy for adenomas is 24.1% while that for smaller and flat or sessile polyps is significantly higher[4]. For the sensitive diagnosis of colorectal cancer lesions, advanced molecular imaging techniques, such as fluorescence endoscopy targeting tumor-specific molecules, have been developed[5–7]. Fluorescence-based tumor imaging can be a useful technique for early cancer detection owing to its advantages of high specificity and sensitivity, real-time imaging, and the absence of radiation exposure[8]. In previous studies, a fluorescence-labeled compound, which could bind to tumor-specific molecules, such as vascular endothelial growth factor (VEGF)[9,10], epidermal growth factor receptor (EGFR)[11], colon cancer specific protein-2 (CCSP-2)[12], endothelial A receptor (ET_AR)[13], c-Met[14,15], etc. was developed to detect colon cancer. Although various probes have been used, their safety in the human body and their ability to detect precancerous lesions, such as adenoma, serrated polyps, and dysplasia, must be confirmed before applying this technology in clinical endoscopic examination[16].

Indocyanine green (ICG) is a fluorescent contrast agent approved for clinical applications in the USA and some European and Asian countries, with a great safety profile for hepatic function examinations[17,18].

Based on the preferred chemical properties for *in vivo* imaging, various clinical and preclinical applications have been reported, including tumor detection in the liver[19,20], breast[21], head and neck[22], lungs[23], ovaries[24], and colon[25,26] of humans using ICG. Despite little background noise in the gastrointestinal tract under near infrared light exposure with ICG fluorescence endoscopy[27], verification of the practicality of ICG injection to detect colon cancer and pre-cancerous lesion in the clinic has been insufficient.

To verify the feasibility of ICG for clinical endoscopy, we investigated the correlation coefficient of fluorescence intensity with tumor stage and colon cancer specific targets in a colitis-associated colon cancer model. Further, we evaluated the mechanism of ICG retention in tumor cells and its relation with iNOS expression using a cell culture experiment and validated the correlation of fluorescence intensity and malignant lesion in patient tissues.

Results

Induction of colitis-associated colon cancer in mice and fluorescence endoscopy imaging with ICG

Colitis-associated colon cancer was induced in 14 mice using Azoxymethane (AOM)/ Dextran Sodium Sulfate (DSS). After a second introduction of DSS, all mice were monitored every week with endoscopy, and various size and phase of proliferative lesions were observed (Fig. S1). At monitoring week 5–6, the colon of all mice was observed, which revealed multiple tumor polyps that were identified as dysplasia, adenoma, and carcinoma via histological analysis (Fig. 1A). After 30 minutes from the ICG injection, fluorescence signal of most polyps was increased with low background, whereas colon of normal mouse showed little signal in both real time fluorescence endoscopy and *ex vivo* molecular imaging (Fig. 1A, S2). To examine the quantitative analysis of ICG molecular imaging of tumor growth, the fluorescence intensity value of the region of interest (ROI) of 25 tumor lesion and their adjacent normal lesion was quantified from real time fluorescence endoscopy and *ex vivo* molecular imaging. Most polyps were detected to have various ICG fluorescence intensity values, which significantly increased compared to those of normal lesions in real time fluorescence endoscopy and *ex vivo* molecular imaging (Fig. 1B, C). For the endoscopy ICG fluorescence intensity values, the average ICG signals of dysplasia, adenoma, and carcinoma were 1.8-fold, 2.8-fold, and 3.1-fold higher than that of the normal lesion (Table 1). For distinct detection cases with 1.5-fold higher intensity than the normal lesions were analyzed for real time fluorescence endoscopy; all carcinoma lesions had more than 2-fold higher intensity. Further, 90% (9/10 cases) of adenoma and 57.1% (4/7 cases) of dysplasia were found to have more than 1.5-fold higher fluorescence intensity than the adjacent normal lesion via real time fluorescence endoscopy (Table 1, S2).

Table 1. Visualization percentages of pre-cancerous lesions using ICG fluorescence endoscopy

	Dysplasia	Adenoma	Carcinoma
Tumor/Normal	1.76 ±0.71	2.84 ±1.78	3.10 ±1.31
% cases > 1.5-fold	57.1 (4/7)	90 (9/10)	100 (9/9)

Correlation analysis of fluorescence intensity and molecular targets for tumor imaging

For precise analysis of tumor status and ICG fluorescence intensity, we calculated the correlation of fluorescence intensity values, histology, and tumor specific molecules used for molecular imaging of colon cancer. A total of 25 polyps and 5 normal tissues from 14 AOM/DSS mice were examined for correlation analysis (Fig. 2A, Fig. S4). Immunohistochemistry of proliferative cancer specific, vascular targeting, inflammatory molecules, including c-Met, Ki-67, VEGFA, CD31, and iNOS, were scored based on an inspection by a pathologist and references (Fig. 2B, Fig. S4)[18,28,29]. As shown in Fig. 2c, the ICG fluorescence intensity was positively correlated with Ki-67, c-Met, and iNOS. The correlation coefficient of CD31 with ICG intensity of real time fluorescence endoscopy was 0.447, whereas that with *ex vivo* molecular imaging was 0.144 (Fig. 2D, E). Further, the correlation coefficient of VEGFA with ICG fluorescence intensity of real time fluorescence endoscopy was 0.250, whereas that with *ex vivo* molecular imaging was 0.439 (Fig. 2D, E). The CD31 expression of tumor tissue was higher than that of normal tissues; however, the immunohistochemistry (IHC) score was relatively low compared to that of other molecules and no differences were found according to tumor growth (Fig. 2F). VEGFA expression was found to increase in adenoma and carcinoma, while basal expression was identified in normal tissue and dysplasia. c-Met, Ki-67, and iNOS had higher IHC scores for dysplasia than normal and the highest IHC scores were found for carcinoma, which was consistent with the ICG fluorescence intensity (Fig. 2F

Cellular nitric oxide concentration is related to the preferential accumulation of ICG in tumor

To elucidate the mechanism of higher detection of ICG in malignant lesions, we examined ICG accumulation in cultured cells according to time. As shown in Fig. 3A, the ICG signal of SW480 and HCT116 was significantly higher than that in the normal colon epithelial cell line CCD841 until 18 h after treatment. As described previously, there was no change in cell viability according to the time of ICG treatment (Fig. S5). The cellular expression of Ki-67, VEGFA, c-Met, and iNOS also increased in SW480 and HCT116, whereas no expression was found in CCD841 (Fig. 3B). Cellular nitric oxide is related to the inhibition of drug efflux[30]. After ICG treatment for 30 min, the intracellular concentrations of nitric oxide in SW480 and HCT116 were significantly higher than that in CCD841 ($p < 0.0005$, Fig. 3C). To verify the

inhibition of efflux protein, ABCB1 (p-gp) expression was checked by immunoblotting, as shown in Fig. 3D, ABCB1 was down regulated after treatment of ICG for 30 min in cancer cell lines.

ICG molecular imaging for colorectal cancer patients

We analyzed the correlation of ICG fluorescence intensity and iNOS and c-Met expression using 16 samples from 8 patients with colorectal cancer (Table 2) via *ex vivo* molecular imaging. After 30 min from ICG injection, the fluorescence intensity and iNOS expression of tumor and normal tissues were measured (Fig. 4A, Fig. S6). As shown in Fig. 4b, the ICG fluorescence signals of tumor tissues were significantly higher than those of normal tissues ($p = 0.0003$). Further, the iNOS expression of tumor tissues was increased compared to that of normal tissues and was positively correlated with the ICG fluorescence intensity ($r = 0.5114$, Fig. 4C). ICG fluorescence signal and iNOS expression in tissue were observed in same location (Fig. 4A). c-Met expression in the tumor was increased as described previously and had a high positive correlation with ICG fluorescence intensity (Fig. S7). To assess the effectiveness of ICG for detecting tumor lesions with increased iNOS expression *in vivo*, orthotopic tumor-bearing mice were evaluated via real time fluorescence endoscopy. Mice with confirmed tumor growth were administered ICG (7.5 mg/kg body weight) via the tail vein. After 30 min, the accumulation of ICG in tumor lesions with minimal autofluorescence background was detected and maintained for 1 h (Fig. 5A). The expression levels of iNOS and c-Met were detected using IHC staining, which revealed increased expression in tumor with high ICG fluorescence signals (Fig. 5B).

Table 2. Clinical information of colorectal cancer patients

Characteristics	No. of patients	%
Sex		
Male	4	50
Female	4	50
Age		
≥55Y	5	62.5
<55Y	3	37.5
Histological grade		
Adenoma	0	0
Well differentiation	0	0
Moderate differentiation	7	87.5
Poor differentiation	0	0
Metastasis		
ND	1	12.5
Lymph node	7	87.5

Discussion

The preferential accumulation of ICG in tumor has been reported for various tumor types, including colon cancer[22,31–33]. However, there are no reports on the potential of ICG-based real time fluorescence endoscopy imaging for pre-cancerous lesions in the clinic. In this study, we investigated the percent

visualization ability of ICG endoscopy in colitis-associated colon cancer using an animal model and patient tissues. All carcinoma lesions could be detected with an average of 3.10-fold higher intensity, further, 90% of adenoma lesions were detected with more than 1.5-fold higher intensity. The ICG intensity clearly correlated with the expression level of c-Met and iNOS, leading to an increase in NO concentration in tumor cells, which was related with down regulation of ABCB1 expression.

Numerous approaches have been employed to detect colorectal cancer lesions using fluorescently labeled antibodies or small molecules binding tumor cell[16]. Fluorescence labeled antibodies against EGFR and VEGF showed high specificity for the targeting tumor; however, these antibodies could not overcome the disadvantages of a longer time to reaction after injection, and immunogenicity[9,11]. For enhanced ability, fluorescence labeled small peptide targeting c-Met was developed[15] and tested in 15 patients via intravenous injection to observe malignant polyps; however, limitations with background signal and low number of cases to confirm safety were reported. In this study, we validated the clinical feasibility of ICG fluorescence endoscopy for tumor detection. ICG has been used in the clinics for more than 40 years[34], thus, it's safety for human body was confirmed. According to some studies, ICG can be applied to detect colon tumors in a colitis-associated colon cancer animal model[18,35]. In the present study, the value for the fluorescence intensity of ICG via real time fluorescence endoscopy and *ex vivo* molecular imaging was quantified, and the correlation coefficient with tumor growth in 25 polyps from animal models and 16 human tissues was calculated. ICG could detect 100% of carcinoma, 90% of adenoma, and 57.1% of dysplasia within 30 min after injection via real-time fluorescence endoscopy.

Ki-67 is a generally used as a marker of proliferation for tumor grading[36,37] and was found to have a positive correlation with ICG intensity ($r = 0.585$) in our real time fluorescence endoscopy experiment. The tumor stage of patient tissues with a high percentage of Ki-67 was T4 whereas that of others was T3, as described previously. However, the ICG intensity and Ki-67 were not directly correlated in human patient tumor tissues ($r = 0.025$). As all patient samples were surgical carcinoma tissues, the ICG intensity could distinguish between normal and carcinoma tissues rather than cancer grades. The ICG fluorescence intensity of tumor was clearly correlated with c-Met expression in animal model and patient tissues ($r = 0.443$ and $r = 0.759$, respectively). c-Met has been considered to be a suitable biomarker for early stages of cancer, including adenoma[15,38]. Recently, cyanine dye (Cy5) labeled peptide probe has been tested for fluorescence endoscopy detection in 15 colorectal cancer patients, and this peptide probe could detect most adenomatous polyps as well as more than half of hyperplasia[15]. These are consistent with our correlation data of ICG fluorescence intensity in animal model. Meanwhile, our data revealed that ICG intensity highly correlated with iNOS expression in the colitis-associated colon cancer mouse model and tissues from colorectal cancer patients ($r > 0.5$). In fact, the expression of iNOS was demonstrated to be associated with poor survival in several cancers[39–41] and is upregulated in most chronic inflammatory disease and cancers, including ulcerative colitis and colon cancer[42]. Tumor cellular iNOS contributes to the production of nitric oxide in the presence of NADPH and oxygen. In recent studies, an increase in nitric oxide concentration was shown to mediate drug efflux inhibition by inactivating ATP binding cassette (ABC) transporters, such as ABCB1 (P-gp), ABCC1 (MRP1) and ABCG2 (BCRP) in tumor cells[43–45].

Although previous studies have demonstrated that preferential ICG uptake is due to extravasation and endocytosis[46], the mechanism of tumor selective retention is poorly understood. Based on the *in vitro* data of the present study, concentration of cancer cellular ICG according to time differed from those of normal colon epithelial cells, and iNOS expression and intracellular nitric oxide concentration level of cancer cell was higher. We also observed the expression of ABCB1 was down regulated in cancer cells after ICG treatment for 30 min. These results suggest that increased cellular nitric oxide concentration caused differences in ICG efflux compared to that in normal cells, resulting in prolonged retention in the short term (in 24 h). Indeed, a prior report revealed that the increase in nitric oxide concentration and iNOS expression was associated with a marked reduction in the doxorubicin efflux rate in colon cancer cell lines[30]. The correlation coefficient of ICG fluorescence intensity of tumor and vascular targeting molecules, including VEGF (r = 0.250) and CD31(r = 0.447), was relatively low, which suggests that the tumor selectivity of ICG is related to an increase in vascular permeability rather than an angiogenic effect. Vascular permeability is promoted by inflammatory mediators, such as iNOS[47], which was highly correlated with ICG intensity as per our correlation analysis data.

In this study, we demonstrated that ICG could be employed for carcinoma and adenoma imaging in colitis-associated colon cancer patients. However, this study has some limitations. Of note, a small sample number without adenoma cases could limit the universality of the results. Thus, the feasibility of ICG in detecting pre-cancerous lesions in a larger cohort needs to be investigated.

In conclusion, we proved the feasibility of ICG as a detector of pre-cancerous lesion via real time fluorescence endoscopy and positive correlation of ICG intensity and expression of c-MET and iNOS in patient tumor tissues. Furthermore, we suggested the mechanism that intracellular iNOS concentration is related to ICG retention in cancer cells.

Materials And Methods

Patient consent for human participants

All patient tissues and data used in this study were provided by the Institutional Review Board of Asan Medical Center (IRB; protocol No. 2017 – 0837). Comprehensive approvals for basic research were obtained from all patients, and informed consent was obtained from all subjects and/or their legal guardian(s). This study was conducted in accordance with the Ethical Guidance of the Declaration of Helsinki.

Animal study ethics

All animal studies were approved by Institutional Animal Care and Use Committee of the Asan Institute for Life Sciences, Asan Medical Center (IACUC; Approval No. 2019-12-205). All animal care and experimental procedures aligned with appropriate instructions and regulations of the Institutional Animal Care and Use Committee (IACUC) at Asan Medical Center and ARRIVE guidelines.

Cell lines

The human colon cancer cell lines, HCT116, SW480, and CCD841, were obtained from the American Type Culture Collection (ATCC; Manassas, VA, USA). Cells were maintained in DMEM/HIGH GLUCOSE (Gibco; Thermo Fisher Scientific, Inc., Waltham, MA, USA) supplemented with 10% fetal bovine serum (Hyclone, Logan, UT, USA) and 1% Antibiotic-Antimycotic (Gibco; Thermo Fisher Scientific, Inc.). The cell lines were grown at 37°C in a humidified incubator containing 5% CO_2.

Establishment of the AOM/DSS-induced colitis-associated colon cancer mouse model

Male Balb/c mice (age, 6–7-week-old; weight, 20–23 g) were purchased from Orient Bio (Seongnam, South Korea). Starting from 7-to 8-weeks old, mice were administered a single intraperitoneal injection of AOM (10 mg/kg body weight; Wako Pure Chemical Co., Osaka, Japan). One week after the AOM injection, colitis was induced by two intermittent one-week-cycle administration of 2% dextran sodium sulfate (DSS; MP Biochemicals, Santa Ana, CA, USA) in drinking water. Mice that showed critical weight loss during the 1 week of DSS administration had their DSS treatment discontinued immediately. One week after discontinued DSS administration, tumor progression was confirmed weekly through fluorescent colonoscopy (Vetcom; Karl Storz, Tuttlingen, Germany).

Orthotopic colonic submucosal implantation of colorectal cancer cells

Before orthotopic submucosal injection was performed, a fabricated needle was prepared for the working channel of the colonoscopy (Vetcom; Karl Storz). A 30G needle was bound to a 23G needle with a flexible plastic pipe. Thereafter, 1×10^7 HCT116 and SW620 cells in 50–100 μL of 10% Matrigel (Corning)/phosphate buffered saline (PBS) were injected into 8–10-week-old balb/c mice (Orient Bio Inc.). A colonic submucosal injection was gently inserted into the working channel of the endoscope using the modified flexible needle. After injection, tumor formation was confirmed through colonoscopy imaging every week. Colonoscopy was performed using fluorescence colonoscopy (Vetcom; Karl Storz).

Real-time fluorescence endoscopy imaging of mouse colon tumor

ICG was purchased from USP (1340009, USP, Rockville, MD, USA). All colonoscopies were performed using the animal endoscopic system (Vetcom; Karl Storz). The IMAGE1 H3-ZF1 THREE-CHIP FULL HD Camera system with fluorescent filters (wavelengths 805–835) that enable ICG fluorescence detection in the basic endoscope and the modified D-light PVET source (66100M3) were added. All endoscopy images were recorded as mp4-video files using the AIDA HD control system (Karl Storz) and sequences of endoscopy images were converted into TIF images through snapshot. The endoscopy image fluorescence intensity was analyzed by ImageJ (NIH, Bethesda, MD, USA). ROIs were defined around the detected polyp according to the corresponding bright-field images. Thereafter, ROIs of polyps were

compared to adjacent normal mucosa and documented as a tumor-to-normal ratio for each site. After tumor implantation, orthotopic mice were administered ICG via tail vein injection. Thirty minutes later, endoscopy was performed and images were obtained with the animal endoscopic system (Vetcom; Karl Storz). To confirm the intensity of fluorescence detection in *ex vivo*, molecular imaging was performed using the Xenogen IVIS spectrum system (Caliper Life Sciences, Inc., Hopkinton, MA, USA).

Ex vivo molecular imaging of CRC patients

Human colon tissues (10–20 mm) were surgically excised from eight patients. Each fresh CRC tissues with adjacent normal colon tissues were evaluated immediately following surgery. Autofluorescence images of the tumor tissues and paired normal colon tissues were obtained prior to ICG incubation. Before incubation, to prevent possible false-positive effect from probe infiltration of the resection, the tissue was covered with low–melting agarose gel. CRC tissues and paired normal colon tissues were incubated with ICG (5 mg/mL) for 30 min. After incubation, tissues were washed three times with PBS, and fluorescence molecular imaging was performed with the Xenogen IVIS spectrum system (Optix MX3 system; ART Advanced Research Technologies Inc., Montreal, Canada).

Histology and immunohistochemistry

Immunohistochemistry was performed using patient colon tissues, which were fixed with 4% paraformaldehyde and embedded in paraffin. Immunostaining was performed using the BenchMark XT automatic immunostaining device (Ventana Medical Systems, Inc., Oro Valley, AR, USA) and OptiView DAB IHC Detection (Ventana Medical Systems, Inc.). Tissue sections (4 μm) were transferred to salinized, charged slides and incubated at room temperature and 65°C. After antigen retrieval for 64 min, the sections were incubated on a fully automated immunostainer with anti-iNOS antibody (Abcam, Cambridge, UK; ab178945) for 32 min. Tissue section slides were then counter-stained with DAPI. All image staining patterns of the slides were acquired using an OptiView DAB IHC Detection Kit (Ventana Medical Systems, Inc.,). Further, all images were acquired using an x20 objective lens.

Immumofluorescence

Tissue cryosection fixed with 4% paraformaldehyde were incubated with the iNOS antibody, followed by incubation with anti-rabbit IgG Alexa Fluor ^{TM} 488 (Thermo Fisher Scientific). Microscopic observation images were obtained by using ZEISS Axio Observer (Zeiss, Oberkochen, Germany).

Detection of time-based ICG accumulation in vitro

The tested cell lines (HCT116, SW480, and CCD841) were seeded in 96-well plates at a density of 1×10^4 cells per well. The cells were incubated with ICG (50 μM) for various durations (0, 1, 5, 10, 20, 30, 60 min and 12, 18, 24 h) at 37°C. To confirm the intensity of ICG accumulation *in vitro*, fluorescence molecular imaging was performed using the Xenogen IVIS spectrum system (Caliper Life Sciences, Inc.).

Western blot analysis

The cell lysates were prepared with RIPA lysis buffer (Thermo Fisher Scientific, Inc.) and protease inhibitor cocktail (GenDEPOT, Barker, TX, USA). Cell lysates were separated using 10% SDS-PAGE and transferred to PVDF membranes. Protein-transferred membranes were blocked with 5% BSA in Tris-buffered saline Tween 20 (TBS-T) for 1 h at room temperature and incubated with blocking buffer-diluted primary antibodies, including E-cadherin (Abcam; ab76055), iNOS (Abcam; ab178945), c-Met (Abcam; ab51067), VEGFA (Abcam; ab46154), Ki-67 (Abcam; ab16667) or ABCB1 (Abcam; ab170904) antibody (1:1000) at 4°C overnight. After the membranes were washed and incubated with secondary antibodies, immunoreactive protein expression signals were detected using the ECL substrate (Thermo Fisher Scientific, Inc.) and visualized using Luminograph III (ATTO Corporation, Tokyo, Japan). The expression of anti-β-actin (Sigma-Aldrich Co., St. Louis, MO, USA) was used as the loading control.

Intracellular nitric oxide assay

The tested cell lines (HCT116, SW480, and CCD841) were seeded in 96-well plates at a density of 1×10^4 cells per well. Quantification of NOS activity in a 96-well format was performed using the manufacturer's instruction. Briefly, the nitric oxide fluorometric probe in working solution was added to each well and incubated at 37°C in the dark for 2 h. Cell lysis buffer was then added to each well without washing before measurement. The fluorescence intensity at excitation/emission wavelengths of 480/530 nm was measured using a CLARIOstar microplate reader (BMG Labtech, Ortenberg, Hessen, Germany).

Statistical analyses

Data are presented as mean ± standard error of the mean (SEM). Significant differences were evaluated using a paired t-test for compare to intensity of normal between polyps. Correlation analysis and coefficient calculation were performed with GraphPad Prism (GraphPad Software, CA, USA).

Declarations

Acknowledgements: We thank the Scientific Publications Team at Asan Medical Center for their editorial assistance with the preparation of this manuscript and the Asan Medical Center for support and instrumentation.

Author contributions: SYK, SJM conceived and designed the analysis; JHK and HJK performed the experiment and collected the data; YSY, CWK, SMH, SK, JSB, BDY, and SKY contributed the data or analysis tools; DC and JC performed the analysis; and SYK, SJM and JHK wrote the paper.

Data availability: The datasets used and/or analyzed during the current study available from the corresponding author on reasonable request.

Funding: This research was supported by a grant from the Korea Health Technology R&D Project through the Korea Health Industry Development Institute (KHIDI), funded by the Ministry of Health & Welfare, Republic of Korea (grant numbers: HI20C0179 and HR21C0198); and Basic Science Research Program

through the National Research Foundation of Korea (NRF) funded by the Ministry of Education (2021R1A6A1A03040260).

Competing interests: The authors declare no competing interests.

References

1. Bray, F. *et al.* Global cancer statistics 2018: GLOBOCAN estimates of incidence and mortality worldwide for 36 cancers in 185 countries. CA Cancer J Clin **68**, 394–424, doi:10.3322/caac.21492 (2018).
2. Leslie, A., Carey, F. A., Pratt, N. R. & Steele, R. J. The colorectal adenoma-carcinoma sequence. Br J Surg **89**, 845–860, doi:10.1046/j.1365-2168.2002.02120.x (2002).
3. Itzkowitz, S. H. & Yio, X. Inflammation and cancer IV. Colorectal cancer in inflammatory bowel disease: the role of inflammation. Am J Physiol Gastrointest Liver Physiol **287**, G7-17, doi:10.1152/ajpgi.00079.2004 (2004).
4. Kim, N. H. *et al.* Miss rate of colorectal neoplastic polyps and risk factors for missed polyps in consecutive colonoscopies. Intest Res **15**, 411–418, doi:10.5217/ir.2017.15.3.411 (2017).
5. Atreya, R. & Goetz, M. Molecular imaging in gastroenterology. Nat Rev Gastroenterol Hepatol **10**, 704–712, doi:10.1038/nrgastro.2013.125 (2013).
6. Nguyen, Q. T. & Tsien, R. Y. Fluorescence-guided surgery with live molecular navigation–a new cutting edge. Nat Rev Cancer **13**, 653–662, doi:10.1038/nrc3566 (2013).
7. Lee, J. H. & Wang, T. D. Molecular endoscopy for targeted imaging in the digestive tract. Lancet Gastroenterol Hepatol **1**, 147–155, doi:10.1016/S2468-1253(16) 30027–9 (2016).
8. Kobayashi, H., Ogawa, M., Alford, R., Choyke, P. L. & Urano, Y. New strategies for fluorescent probe design in medical diagnostic imaging. Chem Rev **110**, 2620–2640, doi:10.1021/cr900263j (2010).
9. Suo, Y. *et al.* NIR-II Fluorescence Endoscopy for Targeted Imaging of Colorectal Cancer. Adv Healthc Mater **8**, e1900974, doi:10.1002/adhm.201900974 (2019).
10. Miyamoto, Y. *et al.* Epidermal growth factor receptor-targeted molecular imaging of colorectal tumors: Detection and treatment evaluation of tumors in animal models. Cancer Sci **110**, 1921–1930, doi:10.1111/cas.14020 (2019).
11. Goetz, M., Hoetker, M. S., Diken, M., Galle, P. R. & Kiesslich, R. In vivo molecular imaging with cetuximab, an anti-EGFR antibody, for prediction of response in xenograft models of human colorectal cancer. Endoscopy **45**, 469–477, doi:10.1055/s-0032-1326361 (2013).
12. Kim, H. I. *et al.* Biomolecular imaging of colorectal tumor lesions using a FITC-labeled scFv-Ckappa fragment antibody. Sci Rep **11**, 17155, doi:10.1038/s41598-021-96281-z (2021).
13. Mucke, M. M. *et al.* Targeting Mucosal Endothelin-A-Receptor Expression by Fluorescence Endoscopy is Feasible to Detect and Characterize Colitis-Associated Cancer in Mice. Inflamm Bowel Dis **24**, 111–122, doi:10.1093/ibd/izx032 (2017).

14. Burggraaf, J. *et al.* Detection of colorectal polyps in humans using an intravenously administered fluorescent peptide targeted against c-Met. Nat Med **21**, 955–961, doi:10.1038/nm.3641 (2015).
15. Burggraaf, J. *et al.* Detection of colorectal polyps in humans using an intravenously administered fluorescent peptide targeted against c-Met. Nat Med **21**, 955–961, doi:10.1038/nm.3641 (2015).
16. Kashihara, T. *et al.* Recent Advances in Molecular Imaging of Colorectal Tumors. Digestion **102**, 57–64, doi:10.1159/000512168 (2021).
17. Alford, R. *et al.* Toxicity of organic fluorophores used in molecular imaging: literature review. Mol Imaging **8**, 341–354 (2009).
18. Nagahara, R. *et al.* Fluorescence tumor imaging by i.v. administered indocyanine green in a mouse model of colitis-associated colon cancer. Cancer Sci **109**, 1638–1647, doi:10.1111/cas.13564 (2018).
19. Gotoh, K. *et al.* A novel image-guided surgery of hepatocellular carcinoma by indocyanine green fluorescence imaging navigation. J Surg Oncol **100**, 75–79, doi:10.1002/jso.21272 (2009).
20. Ishizawa, T. *et al.* Mechanistic background and clinical applications of indocyanine green fluorescence imaging of hepatocellular carcinoma. Ann Surg Oncol **21**, 440–448, doi:10.1245/s10434-013-3360-4 (2014).
21. Ntziachristos, V., Yodh, A. G., Schnall, M. & Chance, B. Concurrent MRI and diffuse optical tomography of breast after indocyanine green enhancement. Proc Natl Acad Sci U S A **97**, 2767–2772, doi:10.1073/pnas.040570597 (2000).
22. Yokoyama, J. *et al.* A feasibility study of NIR fluorescent image-guided surgery in head and neck cancer based on the assessment of optimum surgical time as revealed through dynamic imaging. Onco Targets Ther **6**, 325–330, doi:10.2147/OTT.S42006 (2013).
23. Okusanya, O. T. *et al.* Intraoperative near-infrared imaging can identify pulmonary nodules. Ann Thorac Surg **98**, 1223–1230, doi:10.1016/j.athoracsur.2014.05.026 (2014).
24. Tummers, Q. R. *et al.* The Value of Intraoperative Near-Infrared Fluorescence Imaging Based on Enhanced Permeability and Retention of Indocyanine Green: Feasibility and False-Positives in Ovarian Cancer. PLoS One **10**, e0129766, doi:10.1371/journal.pone.0129766 (2015).
25. Liberale, G. *et al.* Fluorescence Imaging After Indocyanine Green Injection for Detection of Peritoneal Metastases in Patients Undergoing Cytoreductive Surgery for Peritoneal Carcinomatosis From Colorectal Cancer: A Pilot Study. Ann Surg **264**, 1110–1115, doi:10.1097/SLA.0000000000001618 (2016).
26. Yanagita, T. *et al.* Efficacy of intraoperative ICG fluorescence imaging evaluation for preventing anastomotic leakage after left-sided colon or rectal cancer surgery: a propensity score-matched analysis. Surg Endosc **35**, 2373–2385, doi:10.1007/s00464-020-08230-y (2021).
27. Muguruma, N., Miyamoto, H., Okahisa, T. & Takayama, T. Endoscopic molecular imaging: status and future perspective. Clin Endosc **46**, 603–610, doi:10.5946/ce.2013.46.6.603 (2013).
28. Tanaka, Y. *et al.* Effects of growth arrest and DNA damage-inducible protein 34 (GADD34) on inflammation-induced colon cancer in mice. Br J Cancer **113**, 669–679, doi:10.1038/bjc.2015.263

(2015).

29. Pan, Q. *et al.* Genomic variants in mouse model induced by azoxymethane and dextran sodium sulfate improperly mimic human colorectal cancer. Sci Rep **7**, 25, doi:10.1038/s41598-017-00057-3 (2017).
30. Riganti, C. *et al.* Nitric oxide reverts the resistance to doxorubicin in human colon cancer cells by inhibiting the drug efflux. Cancer Res **65**, 516–525 (2005).
31. Martirosyan, N. L. *et al.* Use of in vivo near-infrared laser confocal endomicroscopy with indocyanine green to detect the boundary of infiltrative tumor. J Neurosurg **115**, 1131–1138, doi:10.3171/2011.8.JNS11559 (2011).
32. Holt, D. *et al.* Intraoperative near-infrared imaging can distinguish cancer from normal tissue but not inflammation. PLoS One **9**, e103342, doi:10.1371/journal.pone.0103342 (2014).
33. Kosaka, N., Mitsunaga, M., Longmire, M. R., Choyke, P. L. & Kobayashi, H. Near infrared fluorescence-guided real-time endoscopic detection of peritoneal ovarian cancer nodules using intravenously injected indocyanine green. Int J Cancer **129**, 1671–1677, doi:10.1002/ijc.26113 (2011).
34. Desmettre, T., Devoisselle, J. M. & Mordon, S. Fluorescence properties and metabolic features of indocyanine green (ICG) as related to angiography. Surv Ophthalmol **45**, 15–27, doi:10.1016/s0039-6257(00)00123-5 (2000).
35. Onda, N. *et al.* Fluorescence contrast-enhanced proliferative lesion imaging by enema administration of indocyanine green in a rat model of colon carcinogenesis. Oncotarget **8**, 90278–90290, doi:10.18632/oncotarget.21744 (2017).
36. Menon, S. S., Guruvayoorappan, C., Sakthivel, K. M. & Rasmi, R. R. Ki-67 protein as a tumour proliferation marker. Clin Chim Acta **491**, 39–45, doi:10.1016/j.cca.2019.01.011 (2019).
37. Sobecki, M. *et al.* Cell-Cycle Regulation Accounts for Variability in Ki-67 Expression Levels. Cancer Res **77**, 2722–2734, doi:10.1158/0008-5472.CAN-16-0707 (2017).
38. Di Renzo, M. F. *et al.* Overexpression and amplification of the met/HGF receptor gene during the progression of colorectal cancer. Clin Cancer Res **1**, 147–154 (1995).
39. Ekmekcioglu, S. *et al.* Tumor iNOS predicts poor survival for stage III melanoma patients. Int J Cancer **119**, 861–866, doi:10.1002/ijc.21767 (2006).
40. Lagares-Garcia, J. A. *et al.* Nitric oxide synthase as a marker in colorectal carcinoma. Am Surg **67**, 709–713 (2001).
41. Wang, J. *et al.* Inducible nitric oxide synthase enhances disease aggressiveness in pancreatic cancer. Oncotarget **7**, 52993–53004, doi:10.18632/oncotarget.10323 (2016).
42. Ohshima, H., Tazawa, H., Sylla, B. S. & Sawa, T. Prevention of human cancer by modulation of chronic inflammatory processes. Mutat Res **591**, 110–122, doi:10.1016/j.mrfmmm.2005.03.030 (2005).
43. El-Awady, R. *et al.* The Role of Eukaryotic and Prokaryotic ABC Transporter Family in Failure of Chemotherapy. Front Pharmacol **7**, 535, doi:10.3389/fphar.2016.00535 (2016).

44. Sinha, B. K., Bortner, C. D., Mason, R. P. & Cannon, R. E. Nitric oxide reverses drug resistance by inhibiting ATPase activity of p-glycoprotein in human multi-drug resistant cancer cells. Biochim Biophys Acta Gen Subj **1862**, 2806–2814, doi:10.1016/j.bbagen.2018.08.021 (2018).
45. Kim, M., Park, S. C. & Lee, D. Y. Glycyrrhizin as a Nitric Oxide Regulator in Cancer Chemotherapy. Cancers (Basel) **13**, doi:10.3390/cancers13225762 (2021).
46. Onda, N., Kimura, M., Yoshida, T. & Shibutani, M. Preferential tumor cellular uptake and retention of indocyanine green for in vivo tumor imaging. Int J Cancer **139**, 673–682, doi:10.1002/ijc.30102 (2016).
47. Maeda, H. Vascular permeability in cancer and infection as related to macromolecular drug delivery, with emphasis on the EPR effect for tumor-selective drug targeting. Proc Jpn Acad Ser B Phys Biol Sci **88**, 53–71, doi:10.2183/pjab.88.53 (2012).

Figures

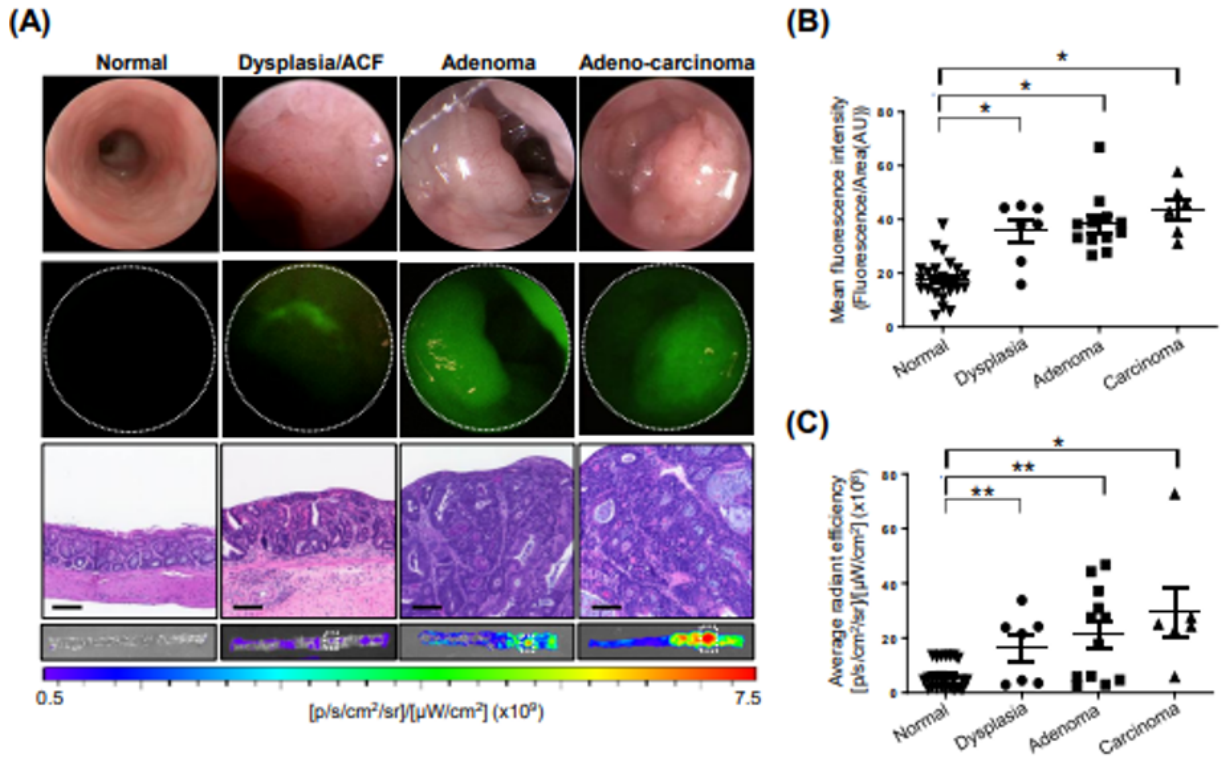

Figure 1

Induction of colitis-associated colon cancer in mice and fluorescence endoscopy imaging with ICG. AOM/DSS-treated mice were intravenously administered ICG. After 30 min, endoscopy was performed. (**A**) Representative endoscopy images of colon adenocarcinoma, adenoma, dysplasia/ACF, and adjacent normal lesion and corresponding H&E-stained images and *ex vivo* molecular imaging of the colon

(magnification, x200, scale bar: 100 μm). (**B**) Mean fluorescence intensity (MFI) of ICG for each type of colon tissue based on the endoscopy images. Values represent mean ± SD. *$p < 0.0001$ (**C**) Quantification of the average radiant efficiency for each type of colon tissue from the *ex-vivo* molecular imaging. Values represent mean ± SD. *$p < 0.0001$, **$p < 0.005$

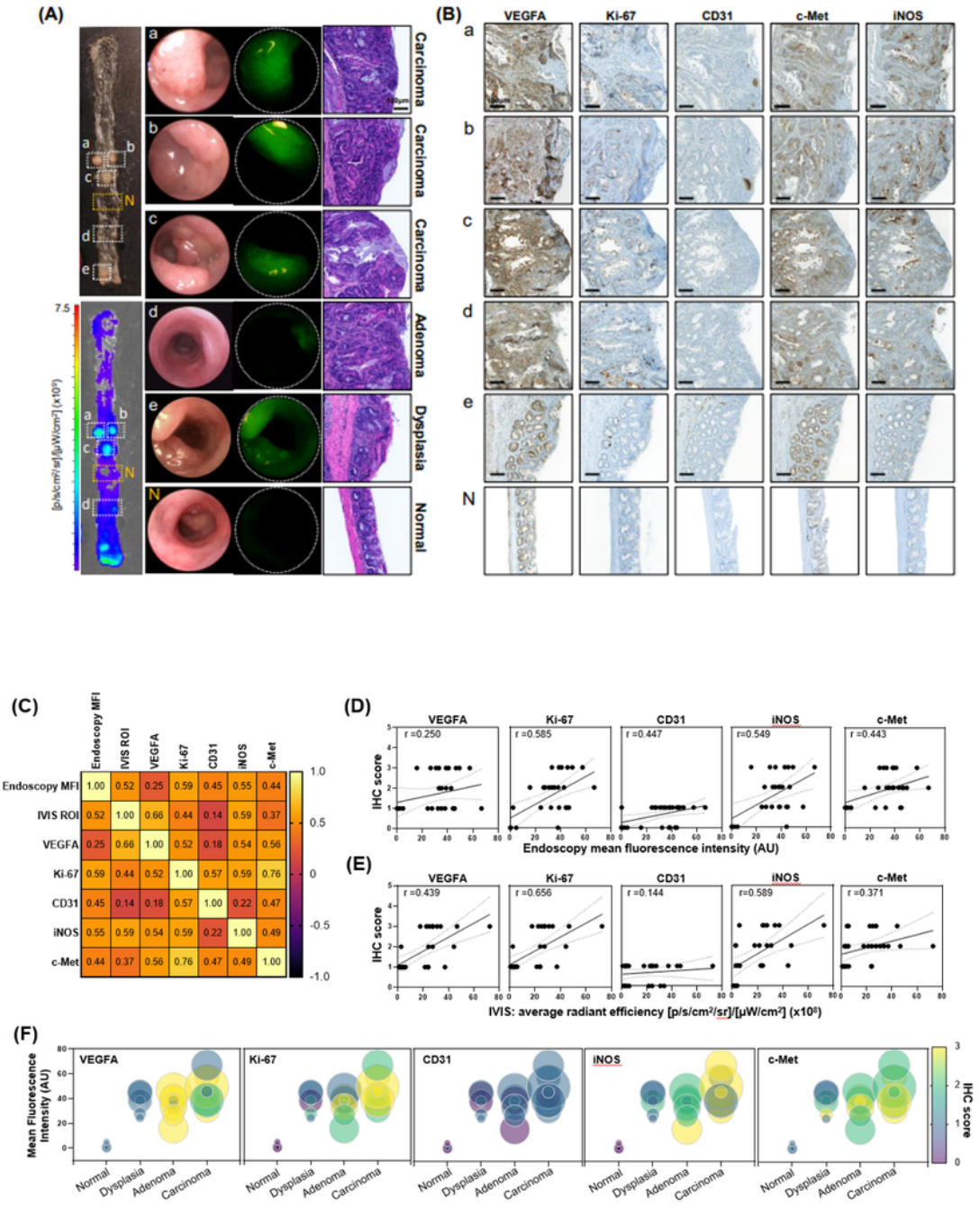

Figure 2

Correlation analysis of fluorescence intensity and molecular targets for tumor imaging. (**A**) Representative ICG fluorescence endoscopy images and *ex-vivo* molecular imaging of polyps and adjacent normal lesions from a mouse colon with the corresponding H&E-stained images (magnification, x200). (**B**) Immunohistochemistry images with VEGFA, Ki-67, CD31, iNOS, and c-Met for the corresponding lesions of (**A**) (Scale bar: 100 μm). (**C**) Heat map for the correlation co-efficient of VEGFA, Ki-67, CD31, iNOS, and c-Met with the endoscopy fluorescence intensity values and the *ex vivo* molecular imaging fluorescence intensity values. (**D**) Correlation analysis between endoscopy fluorescence intensity value (AU) of ICG accumulation and the IHC score of each molecular target. (**E**) Correlation analysis between *ex vivo* molecular imaging fluorescence intensity values of ICG and the IHC score of each molecular target. (**F**) Correlation analysis between ICG intensity values and the IHC score of each molecular targets based on tumor stages. Data are presented as Mean and Error (95% CI). Size of circle, average radiant efficiency from *ex vivo* molecular images ([p/s/cm^2/sr]/[μW/cm^2] (x10^8)).

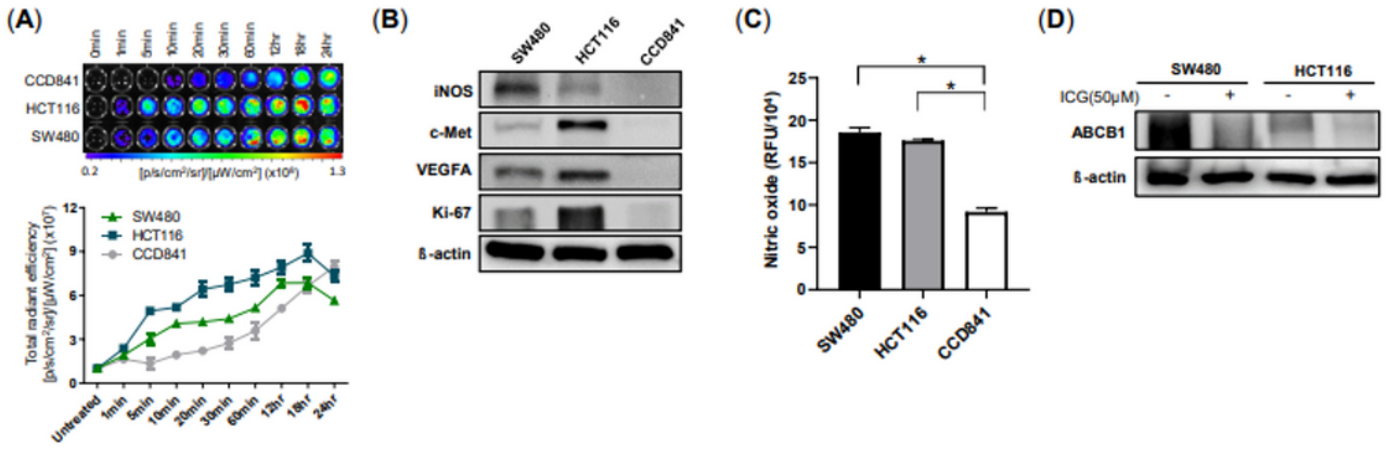

Figure 3

***In vitro* colon cancer cellular accumulation of ICG and iNOS/NO level.** (**A**) Time-based ICG accumulation in a normal cancer cell line (CCD841) and colon cancer cell lines (HCT116 and sw480). A total of 1 × 10^4 cells/well were treated with 50 μM of ICG for 30 min prior to IVIS imaging. (n = 4) (**B**) Western blot analyses of VEGFA, Ki-67, iNOS, and c-Met in SW480, HCT116, and CCD841. (**C**) Intracellular nitric oxide (NO) assessment in SW480, HCT116, and CCD841 cells. Values are expressed as mean ± SEM (*p < 0.05) (**D**) Western blot analyses of ABCB1 in SW480 and HCT116 with treatment of ICG for 30 min.

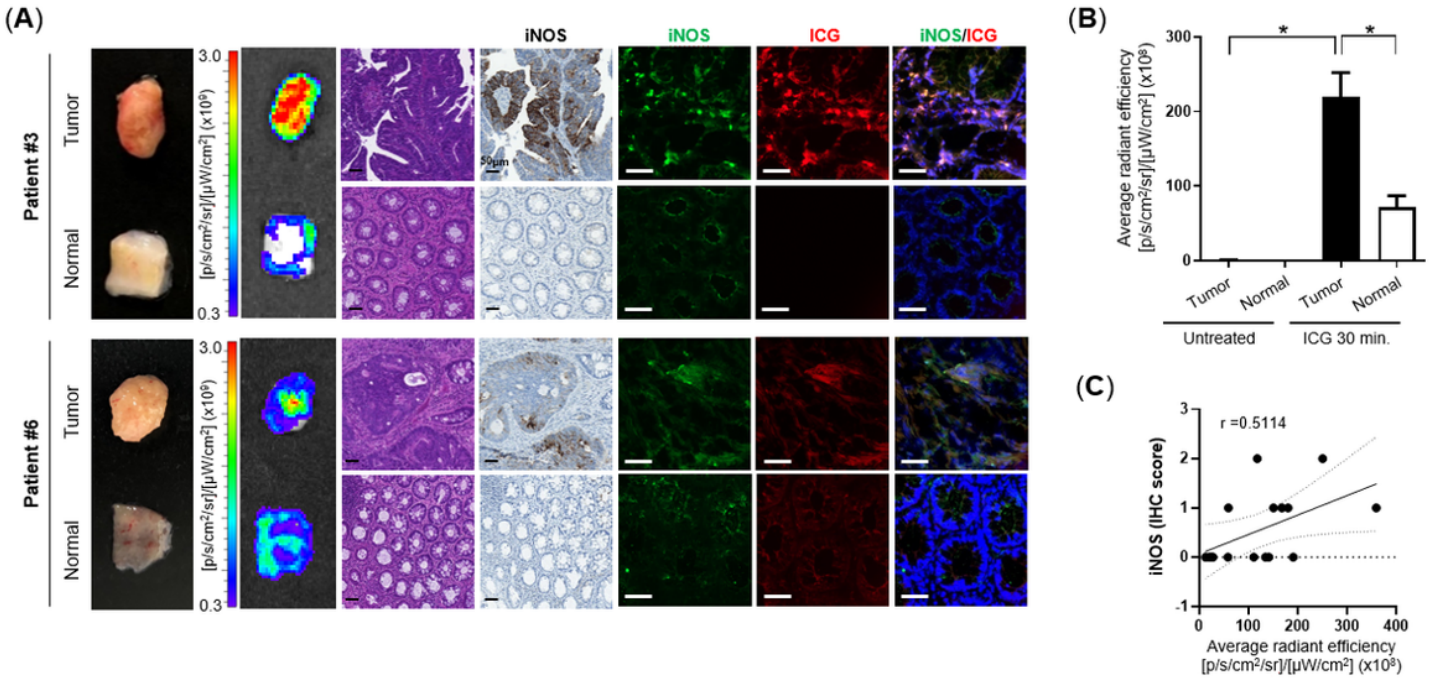

Figure 4

***Ex vivo* molecular imaging of tumor tissues from colorectal cancer patients.** (**A**) Representative *ex vivo* IVIS imaging, H&E, immunohistochemistry, and immunofluorescence images of colorectal cancer patient tissues with strong (upper panel) and weak (bottom panel) intensity of ICG. (Scale bar: 50 μm) (**B**) Average fluorescence intensity of colorectal cancer patient specimen treated with ICG (*$p < 0.05$). (**C**) Correlation analysis between ICG fluorescence intensity value (average radiant efficiency) and the IHC score of iNOS expression in colorectal cancer patient tissues.

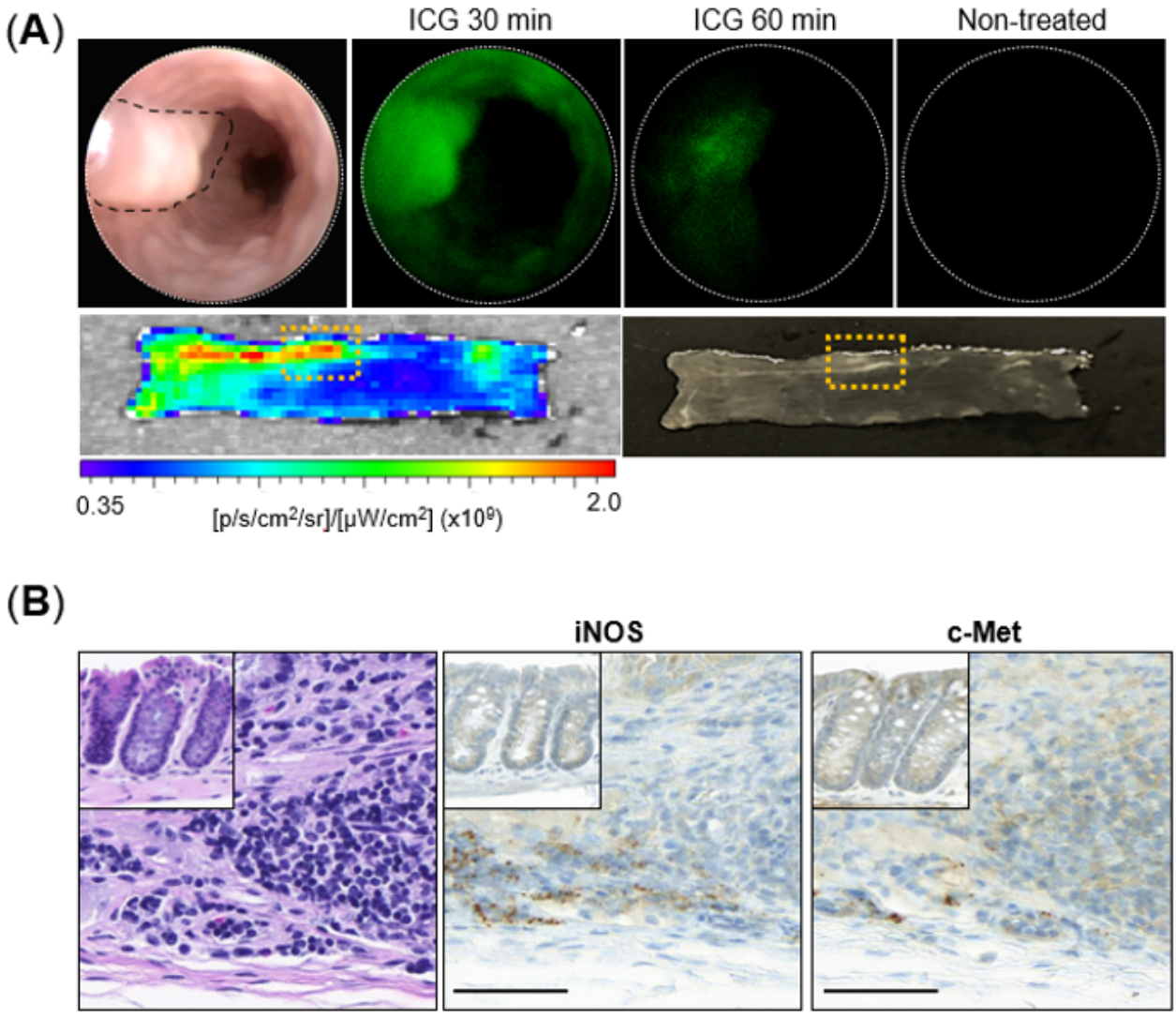

Figure 5

Feasibility assessment of ICG fluorescence endoscopy of colorectal cancer in an orthotopic mouse model. (**A**) Fluorescence endoscopy images showing cancer growth following orthotopic injection of the SW620 cell line with minimal background compared to normal lesion in balb/c mouse. Images were obtained 60 min after the i.v. injection of ICG. Real-time brightfield image of the tumor lesion was acquired. (**B**) Histology and immunohistochemistry of iNOS and c-Met in orthotopic tumor tissues. The inner square shows the adjacent normal colon tissues (Scale bar: 50 μm).

Supplementary Files

This is a list of supplementary files associated with this preprint. Click to download.

- Suppplementaryfigurefinal053022.pdf